4

Journal of Vestibular Research, Vol. 3, pp. 141–161, 1993
Printed in the USA.

0957-4271/93 $6.00 + .00

A MULTIDIMENSIONAL MODEL OF THE EFFECT OF GRAVITY ON THE SPATIAL ORIENTATION OF THE MONKEY

Daniel M. Merfeld,* Laurence R. Young,* Charles M. Oman,* and Mark J. Shelhamer†

*The Man-Vehicle Laboratory, Massachusetts Institute of Technology, Cambridge, Massachusetts;
†The Johns Hopkins University, School of Medicine, Baltimore, Maryland
Reprint address: D.M. Merfeld, Ph.D., The Man-Vehicle Laboratory, Massachusetts Institute of Technology, Cambridge, MA 02139

☐ **Abstract—A "sensory conflict" model of spatial orientation was developed. This mathematical model was based on concepts derived from observer theory, optimal observer theory, and the mathematical properties of coordinate rotations. The primary hypothesis is that the central nervous system of the squirrel monkey incorporates information about body dynamics and sensory dynamics to develop an internal model. The output of this central model (expected sensory afference) is compared to the actual sensory afference, with the difference defined as "sensory conflict." The sensory conflict information is, in turn, used to drive central estimates of angular velocity ("velocity storage"), gravity ("gravity storage"), and linear acceleration ("acceleration storage") toward more accurate values. The model successfully predicts "velocity storage" during rotation about an earth-vertical axis. The model also successfully predicts that the time constant of the horizontal vestibulo-ocular reflex is reduced and that the axis of eye rotation shifts toward alignment with gravity following postrotatory tilt. Finally, the model predicts the bias, modulation, and decay components that have been observed during off-vertical axis rotations (OVAR).**

☐ **Keywords—spatial orientation; model; vestibulo-ocular reflex; monkey.**

Introduction

Many current models of the vestibulo-ocular reflex (VOR) and spatial orientation are derived from "velocity storage" models (1–3). These models were developed when observations showed that perrotatory and postrotatory nystagmus decayed more slowly than the activity of the first order afferents from the semicircular canals and that nystagmus lasted beyond the visual stimulation [optokinetic afternystagmus (OKAN)]. The velocity storage hypothesis proposed that the same neural process was responsible for OKAN and for the extension of vestibular nystagmus. One model used a single positive feedback loop to prolong the vestibular and optokinetic activity (1), another used two parallel paths (2), including a hypothesized "leaky integrator," while a third used a standard engineering estimation technique (3), a Kalman filter (4).

Robinson (1) theorized that oculomotor responses, such as OKAN, should have a rational purpose. As one example, he suggested that to maintain a compensatory eye velocity during rotation, the brain must have a central estimate of head velocity. In the light, the canal and visual signals might be merged to yield a single central estimate of head velocity with the canals utilized for transient signals and vision for sustained stimulation (5–7). Hain (8) later implemented a three-dimensional velocity storage model and hypothesized that otolith signals modify velocity storage feedback parameters and pass through the velocity storage mechanism. This model relied on specific variations in the system parameters to yield changes in response time constants and to produce an ocular response to translation.

RECEIVED 7 May 1992; REVISED MANUSCRIPT RECEIVED 16 September 1992; ACCEPTED 23 September 1992.

The model proposed by Raphan and colleagues (2,9) accomplished velocity storage through parallel processing of the sensory afference. A direct path, from canal afferents to oculomotor system, induced rapid changes in slow phase eye velocity, while an indirect path included a low-pass filter ("leaky integrator") which stored activity and induced slow changes in eye velocity. This model was generalized to include more than a single dimension of rotation by including three velocity storage elements: one for each dimension in 3-space (10). The integrator leak rate matrix was modified by otolith input (and hence by the orientation of gravitoinertial force). This multidimensional model has been further modified (11) to predict that the eigenvalues and eigenvectors of the response are dependent upon the gravitational field such that the response axis aligns with gravity.

Observer theory and optimal estimation theory have also been used to model spatial orientation. Borah and colleagues (3) implemented a Kalman filter that mimicked a number of experimental findings. By proper choice of parameters, they were able to model responses associated with velocity storage, vection, and the gradual tilt experienced during sustained linear acceleration.

Oman (12) used a related approach by developing a heuristic motion sickness model, posing the solution in terms of observer theory, while retaining the sensory conflict notion of earlier theories (13–20). Oman proposed that the CNS possesses a model of body and sensor dynamics that calculates the measurements expected from the sensors (semicircular canals, otoliths, and so on). The error between the expected sensory afference and the actual sensory afference would be used to steer the central estimate toward the true value.

The mathematical model that we developed is closely related to this heuristic approach. Specifically, this sensory conflict model merges information from various sensory modalities to estimate gravitational "down," linear acceleration, and angular velocity. A feedback schema similar to that used in observer theory is used to drive the estimate of spatial orientation toward the true estimate of orientation.

Simulations showed that the model predicted "velocity storage," since the predicted ocular responses extend well beyond the sensory afference during rotation about an earth-vertical axis. Following postrotatory tilt stimuli, the model predicted a faster decay and a shift in the axis of eye rotation compared to the upright postrotatory response as have been observed (21,22). Finally, the model predicted the bias, modulation, and decay components that have been observed during OVAR stimulation in humans (23,24) and monkeys (25, 26). These results show that the basic concepts that we implemented predict the responses for a number of motion paradigms without requiring model parameters that vary depending upon the sensory stimulation. Furthermore, these emergent properties were not specifically designed into the model.

Like previous modeling efforts (1–3), we assumed that the CNS calculates a central estimate representing angular head velocity, which is not always directly proportional to any single sensory or motor signal. Consistent with previous work, we have called this central estimate "velocity storage." Similarly, experiments have shown that tilt responses and responses to linear acceleration are not directly dependent on the sensory stimulation. For example, constant velocity eccentric rotation introduces a constant tilt of gravitoinertial force. Subjective indications of the vertical eventually align with gravitoinertial force during this paradigm, but this gradual process takes approximately one minute (27). In the meantime the tilted estimate of gravity falls somewhere between true gravity and gravitoinertial force, indicating that the CNS is generating an estimate of tilt that is not directly proportional to the stimuli. A linear VOR has also been reported using similar motion paradigms (28–30). This linear VOR decays to zero somewhat exponentially over the course of approximately one minute, while the centripetal acceleration remains constant. Once again the response is not simply proportional to the sensory stimulation. Since the responses are clearly not directly related to any sensory stimulus, the CNS must be creating central estimates of gravity and acceleration. Consistent with the

previous work on angular velocity, we have called these central estimates "gravity storage" and "acceleration storage." In fact, our contribution lies in the extension of the previous models to include these central estimates, which are used to modify responses to angular velocity and to generate ocular responses to linear translation.

Model Development

This model is based on the organization shown in Figure 1. The sense organs transduce motion stimuli into sensory afference that is processed by the central nervous system (CNS) to yield a central (internal) estimate of spatial orientation. The primary goal of this modeling effort is to determine this estimate of central orientation. However, since we hypothesize that the observed eye movements have the functional purpose of accurately compensating for the central estimate of self motion, we have also predicted the VOR responses.

Neglecting orbital dynamics and eye translation during rotation, full compensation for angular velocity is achieved if the slow phase of the angular VOR response is exactly opposite the central estimate of angular velocity. Full compensation for linear motion is a little more complex. In order for the linear VOR to be fully compensatory, it must vary inversely with target distance, which we fixed at 10 m for all simulations, and be proportional to head velocity (31–33). To calculate linear velocity, the CNS could simply integrate linear acceleration, but it is well known that the CNS performs imperfect integration (34). We included this effect by implementing a low-pass filter with a time constant of 80 seconds. In order to compare the modeling results to the existing VOR data, we further hypothesized that the VOR is the sum of an angular VOR and a linear VOR (22,28–30,35,36).

In order to present an easily testable hypothesis, we state here the one assumption that is unique to the structure and organization of this model. This central assumption is that an internal model of body dynamics and sensory dynamics is utilized by the CNS to predict expected sensory afference. The difference between this expected sensory afference and the actual afference from the sense organs is fed back to the internal model to drive the difference toward zero. The specific implementation is based primarily on observer theory (37), though it is also somewhat loosely based on optimal observer theory (4). Our goal was to determine if this hypothesis and framework (Figure 2) would lead to emergent properties that we did not deliberately build into the model.

In traditional controls applications, the goal is to control some dynamic body such that it reaches a "desired state" (for example, position, velocity, or orientation). "Sensors" are used to measure the "true state" of the body as accurately as possible, but because of sensor limitations (for example, sensory dynamics, inadequate or noisy measurements), the sensors may not provide an adequate indication of the "true state." Therefore, we might need to develop an algorithm to estimate the state of the object more accurately. The algorithm may be as simple as low-pass filtering the measurements from the sensors, but in complicated situations, better methods (for example, observer theory) may be required. Independent of how the "estimated state" is determined, we compare the best estimate of the state with the "desired state" and utilize a "control strategy" to move the actual orientation toward that desired.

Observer theory was created to help solve the state estimation problem by using additional information available to the designer. For example, we may know the sensor limitations and may also know something about the object dynamics. In observer theory, this additional system knowledge is used to create a model (analog or computer) of the object dynamics and a model of the sensor dynamics. When the signal is sent to control the body orientation, a "copy of the control signal" is also sent to the "model of the body dynamics," which yields an "estimated state." This estimate is processed by the "model of sensor dynamics" to yield the "expected sensor signals," which are compared to the "sensor

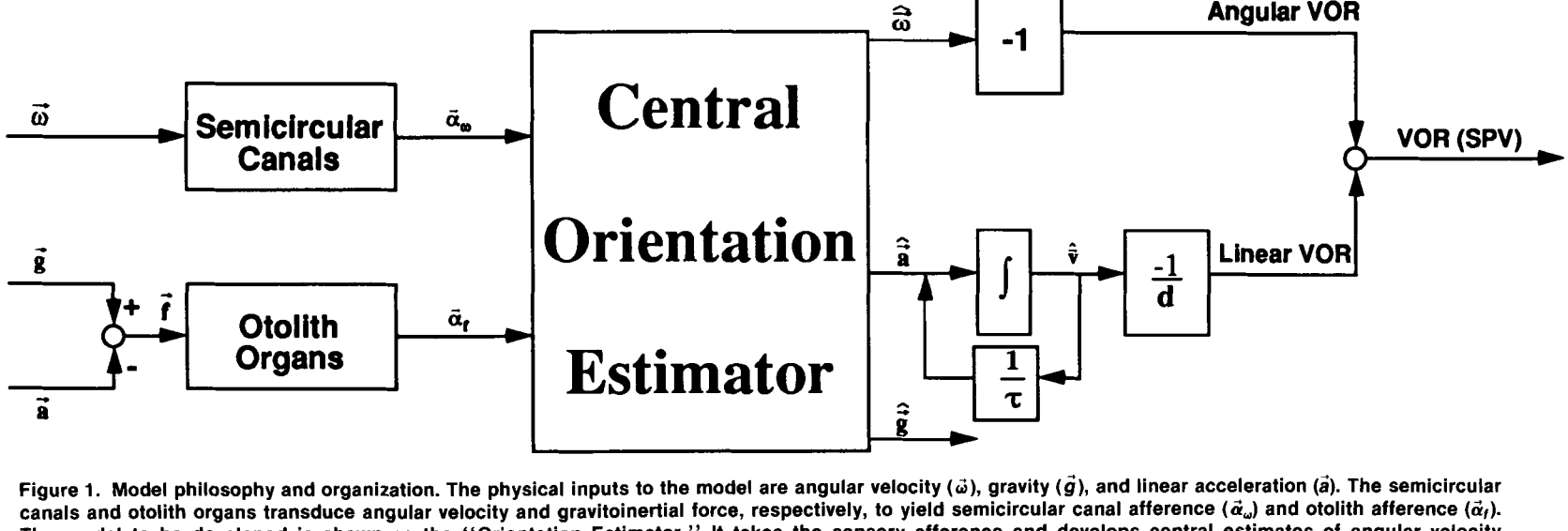

Figure 1. Model philosophy and organization. The physical inputs to the model are angular velocity ($\vec{\omega}$), gravity ($\vec{g}$), and linear acceleration ($\vec{a}$). The semicircular canals and otolith organs transduce angular velocity and gravitoinertial force, respectively, to yield semicircular canal afference ($\vec{\alpha}_\omega$) and otolith afference ($\vec{\alpha}_f$). The model to be developed is shown as the "Orientation Estimator." It takes the sensory afference and develops central estimates of angular velocity ($\hat{\vec{\omega}}$), linear acceleration ($\hat{\vec{a}}$), and gravity ($\hat{\vec{g}}$). The VOR is assumed to be a linear summation of an angular VOR, a compensatory response to a central estimate of angular velocity, and a linear VOR, a compensatory response to a central estimate of linear velocity ($\hat{\vec{v}}$), which is the integral of the central estimate of linear acceleration ($\hat{\vec{a}}$). Because a compensatory linear VOR response has been shown to be inversely proportional to target distance, we have also included a dependence on target distance (d).

signals." The difference is used in a feedback loop to drive the "estimated state" toward the "true state" and minimize the difference in the sensor indications. The only trick requires us to properly design the feedback to make the state estimate converge on the actual state of the object. Linear optimal observer theory (Kalman filtering) provides one method to optimally design this feedback for a linear system, but the nonlinear nature of the model and the time-varying nature of the feedback for a nonlinear model make this theory inappropriate for this application.

Figure 2B is a block diagram that conceptually represents the sensory conflict model in terms of observer theory. "Desired orientation," the primary system input, is compared to the CNS "estimate of orientation" to yield an orientation error. A "control strategy" is applied to the orientation error to yield "efference," which reduces the error. The efferent motor command is relayed to the muscles, which are represented as part of the "body dynamics," to yield the "actual orientation." The actual orientation is measured by the sensory organs with the physiological result being "sensory afference."

The observer portion of the model is incorporated in the lower half of Figure 2B. A copy of the muscle efferent signal, or "efference copy," is sent to an internal model of body dynamics to yield an "estimated orientation." This estimate of orientation is sent to a model of sensory dynamics to generate the "expected sensory afference." The difference between sensory afference and expected sensory afference represents a "sensory conflict." The sensory conflict feeds back on the internal model of body dynamics to steer the estimated orientation toward the true orientation.

We simplified the model by choosing to investigate passive motion only. In most experiments that measure eye movements and/or perceptual responses, the orientation of the subject is directly controlled. Figure 2C shows a restricted version of the model that is appropriate for this condition. The primary system input is now the "external disturbance," which represents the externally controlled orientation of the subject. The rest of the model is identical to the representation shown in Figure 2B, except that portions of the model representing motor control have been eliminated.

We have tried to keep the model as simple as possible, since more complicated models provide extra degrees of freedom, which probably would allow better fits but which may obfuscate the central points of the modeling. As stated before, the goal of this effort was to create a rational model, based on a limited number of physical assumptions, which could mimic the multidimensional responses. Many simplifying assumptions will be briefly discussed in footnotes. These assumptions will not be crucial to understanding the model in a general sense, but will be important for critical readers looking for details.

This model is presented in two stages. First, we develop the model analytically and use a simple scalar example to elucidate the central concepts for a single axis. Then, we develop and simulate multidimensional and multisensory stimulation; postrotational tilt (21), and off-vertical axis rotation (OVAR) (26).

Since there are significant differences between animal and human responses, we needed to pick a single species. Since first order afferents (38,39) and eye movements (21,25,26) have been studied in the monkey, we chose to develop a monkey model as this first step in a long-term modeling project.[1]

One-Dimensional Velocity Storage Model for Upright Yaw Rotation

We chose to begin by simulating upright yaw rotation, which does not include otolith inputs. First, we developed a one dimensional linear model based on the previously outlined assumptions, which provided dynamics indistinguishable from previous models (1,2). The blocks of Figure 2B were replaced by linear transfer functions (Figure 3). The semicircular canals were represented by a high-pass filter with a cut-off frequency equal to the

[1]Parameter changes are presumably required to model other species, including humans. The models for the sensory dynamics may have to be changed, and the four free parameters, to be discussed shortly, may require changes.

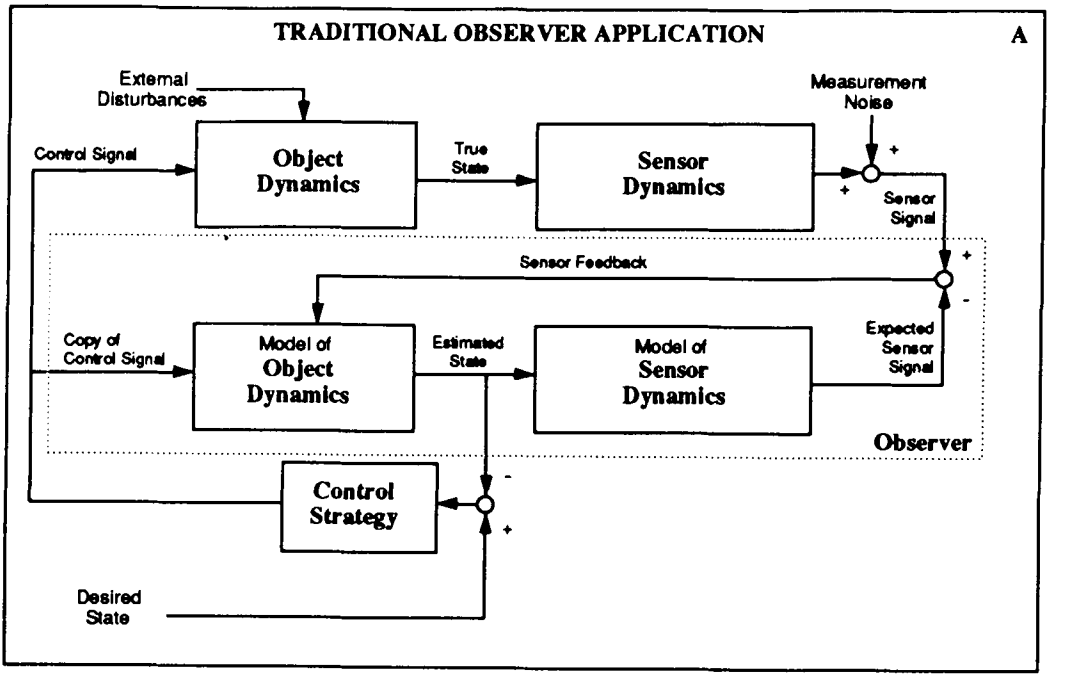

Figure 2. Observer form of sensory conflict model. Figure 2A shows the application of a standard observer. To generate a "control signal," we compare the "desired state" with the "estimated state" and apply a "control strategy" to the difference. The "control signal" and "external disturbances" are processed by the "object dynamics" to yield the "true state," which is measured within the limitations of the "sensor dynamics." The "observer" is used to create the best estimate of the state. A "copy of the control signal" is processed by the "model of object dynamics" to yield the "estimated state," which is processed by the "model of sensor dynamics" to yield the "expected sensory signal." "Sensor feedback" is utilized to make the "estimated state" converge toward the "true state." General form of the sensory conflict model including voluntary control of motion is shown (Figure 2B). Peripheral processes are represented by the blocks labeled "body dynamics" and "sensory dynamics." All other blocks represent processes that are hypothesized to occur centrally. The primary hypothesisis is that the CNS has internal models of the body dynamics and sensory dynamics which it uses to determine an estimate of orientation. Figure 2C is similar to 2B, but shows a simplified version of the model with voluntary control of motion eliminated. This form of the model will be used to predict responses obtained during passive movement of a subject. ***(Figure continues on facing page.)***

inverse of the dominant time constant (τ) of the sensory afference. With this simple representation, a step in angular velocity will result in an exponential decay of the afferent response.[2] Mathematically, the canal transfer function was[3]

$$scc(s) = \frac{\alpha_{\omega_z}(s)}{\omega_z(s)} = \frac{\tau s}{\tau s + 1}, \qquad [1]$$

where α_{ω_z} is the semicircular canal afferent response, ω_z is the angular velocity, s is the Laplace variable, and τ is the dominant time

[2]The afferent responses (α_{ω_z}) are not scaled to represent neural firing rates. They also do not include DC bias or noise. Furthermore, the afferent responses are assumed symmetric about the resting level. Physiological accuracy may be added by including any of these effects with no change in the system output as long as the analogous adjustments are made to the internal model of the sensory dynamics and the feedback gains are adjusted appropriately.

[3]A more complicated third-order transfer function including a time constant to represent adaptation has been determined (38). This more complicated transfer function was included in early versions of the model. We chose to proceed with this simple representation since the predicted responses were not fundamentally altered by this simplification. Physiological accuracy could easily be added by returning to a transfer function more fully representing the dynamics of the semicircular canals.

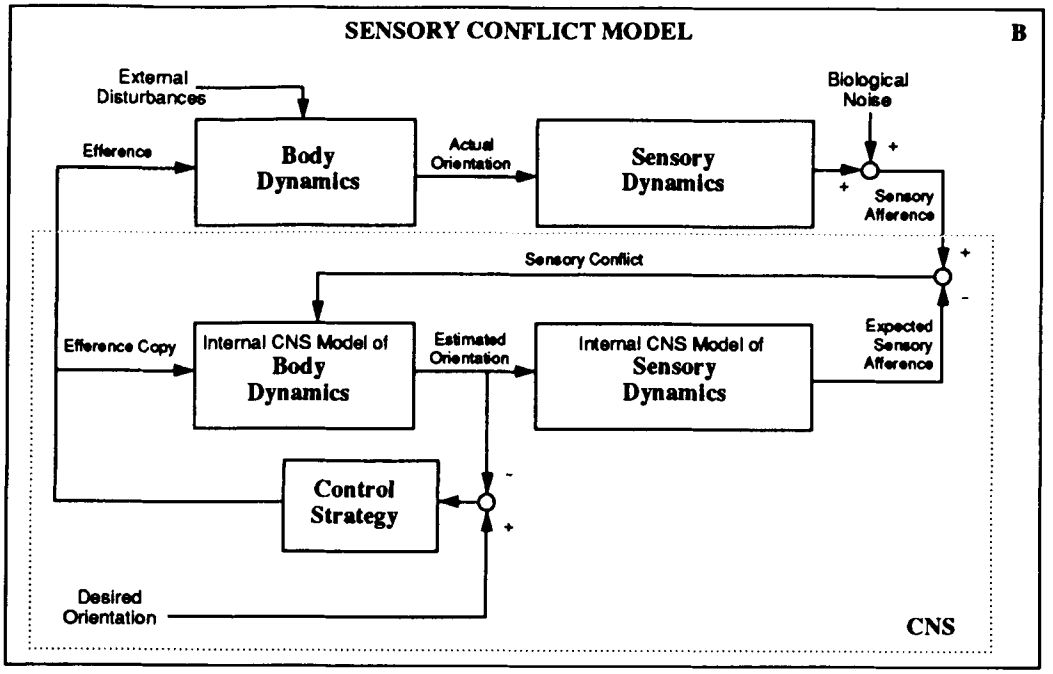

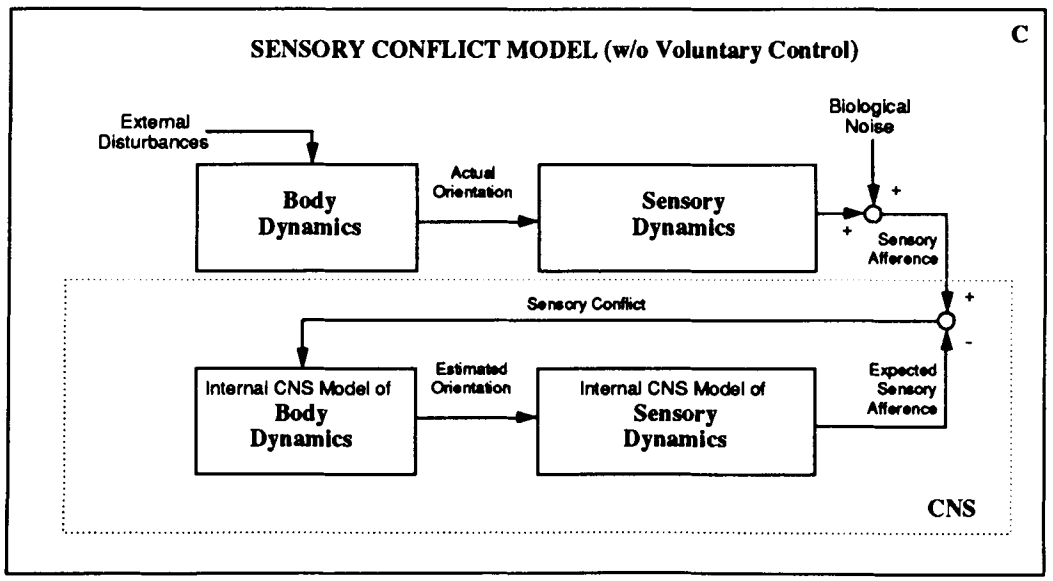

Figure 2 continued.

constant of the semicircular canal. If we assume that the internal model of sensory dynamics has a similar form, we can represent the internal model of sensory dynamics as

$$scc(s) = \frac{\hat{\alpha}_{\omega_z}(s)}{\hat{\omega}_z(s)} = \frac{\hat{\tau}s}{\hat{\tau}s + 1}, \qquad [2]$$

where $\hat{\alpha}_{\omega_z}$ is the expected semicircular canal afference, $\hat{\omega}_z$ is the estimated angular velocity, and $\hat{\tau}$ is the internal model parameter value for the semicircular canal time constant.

Simple algebraic manipulations yield the transfer function from actual angular veloc-

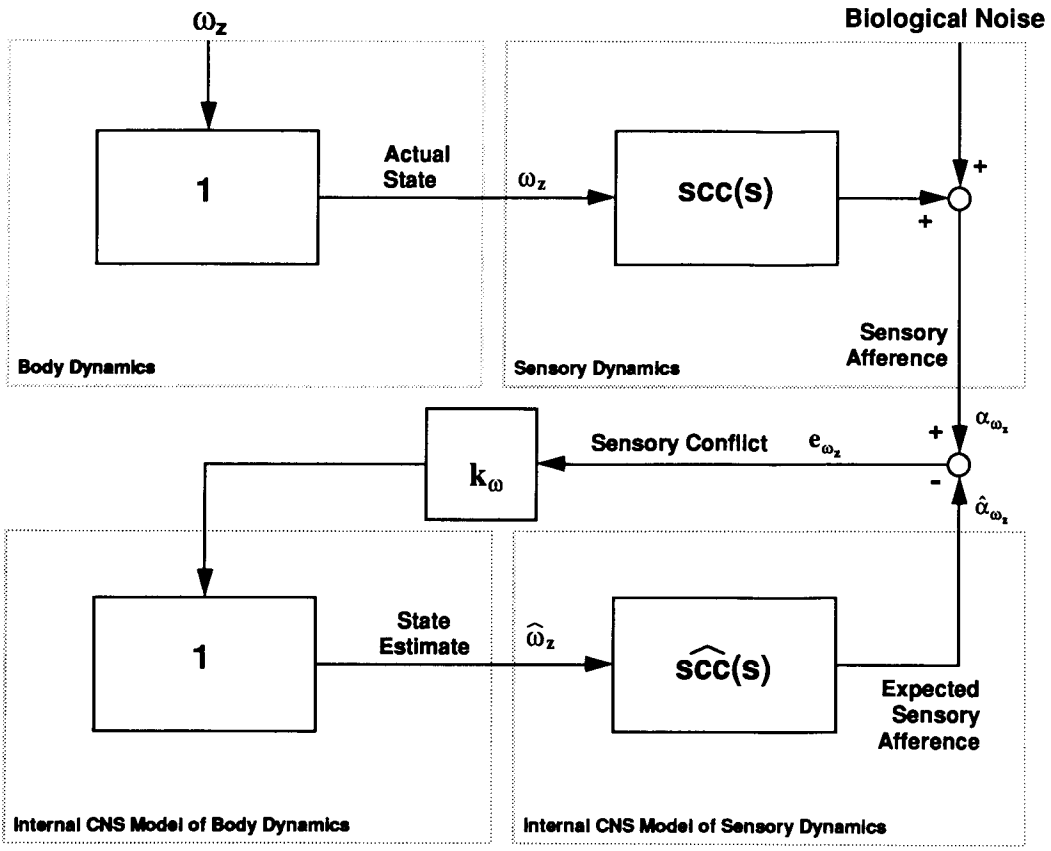

Figure 3. One-dimensional "Velocity Storage" model. Each of the blocks of Figure 2B are replaced by simple linear transfer functions. The sensory dynamics block is replaced by a linear transfer function representing the response characteristics of the semicircular canals. The body dynamics block is replaced by unity since the external angular velocity (ω_z) is also the physical stimulus. Since the purpose of the internal model is to represent the true sensory dynamics and the true body dynamics, the internal model has a form similar to the true dynamics as represented by the bottom half of the figure.

ity (ω_z) to the central estimate of angular velocity ($\hat{\omega}_z$):

$$\frac{\hat{\omega}_z(s)}{\omega_z(s)} = \frac{k_\omega \tau s(\hat{\tau}s + 1)}{((k_\omega + 1)\hat{\tau}s + 1)(\tau s + 1)}. \quad [3]$$

If the actual afferent response and the internal afferent model have the same time constant ($\hat{\tau} = \tau$), a pole-zero cancellation simplifies the transfer function:

$$\frac{\hat{\omega}_z(s)}{\omega_z(s)} = \frac{k_\omega \tau s}{((k_\omega + 1)\tau s + 1)}. \quad [4]$$

This transfer function shows that the central estimate of angular velocity ($\hat{\omega}_z$) has a time constant of

$$\tau' = (k_\omega + 1)\tau, \quad [5]$$

and a gain of

$$G = \frac{k_\omega}{k_\omega + 1}. \quad [6]$$

Figure 4 shows the semicircular canal afferent response and the predicted central estimate of angular velocity for a trapezoidal angular velocity stimulus. The single feedback gain parameter (k_ω) was fixed at 3.0. With a dominant semicircular canal time constant of 5.7 seconds (38), this yields a nystagmus time constant of 22.8 seconds (equation 5) and a gain of 0.75 (equation 6).

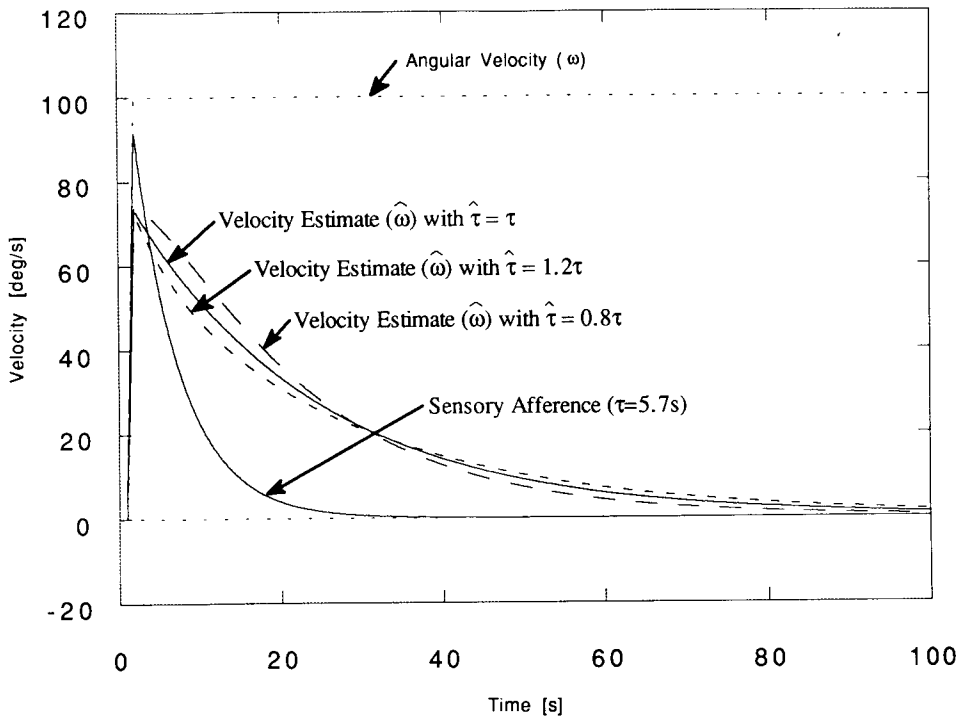

Figure 4. "Velocity Storage" model predictions. Plot shows the semicircular canal afference (τ = 5.7 s) predicted to occur due to the constant velocity yaw trapezoid (ω). The time course of the central estimate of angular velocity is shown with model time constant equal to the time constant of the semicircular canals ($\hat{\tau} = \tau$ = 5.7 s), with the model time constant 20% less than the semicircular canal time constant ($\hat{\tau} = .8\tau$ = 4.56 s), and with the internal model time constant 20% greater than the semicircular canal time constant ($\hat{\tau} = 1.2\tau$ = 6.84 s). Feedback gain (k_ω) was fixed at 3.0 for all simulations.

Note that despite topological differences in the models, equation 3 is similar in form to that of other models (1,2). If $\hat{\tau} = \tau$, this model has a single free parameter (k_ω), which sets both the gain and the time constant. In our model the velocity storage was accomplished by having an internal high pass model of the sensory dynamics as part of a negative feedback loop. This contrasts with the previous models since Robinson (1) used a low-pass filter in a positive feedback loop, while Raphan and colleagues (2) used two parallel paths, a direct path from the afference to the oculomotor response and an indirect path through the "velocity-storage integrator."

To demonstrate that this model is robust to errors in the internal model, we simulated the response with an estimated afferent time constant 20% too large ($\hat{\tau} = 1.2\tau$) and also 20% too small ($\hat{\tau} = 0.8\tau$). Large errors in the model parameters have relatively small effects on the overall system response as demonstrated in Figure 4 where all of the velocity storage responses have qualitatively similar dynamics despite the large differences (±20%) in the internal model semicircular canal time constant.

Multidimensional Sensory Conflict Model

The basic philosophy and assumptions were retained while extending the model to include the otolith organs and also to include "acceleration storage" and "gravity storage," central estimates analogous to angular "velocity storage" in the one-dimensional model. However, some changes were required. First, we defined a head-fixed, right-handed coordinate system such that the x-axis aligns with the naso-occipital axis, the y-axis aligns with

the interaural axis, and the z-axis is perpendicular to the x- and y-axes. The positive direction for the x-axis is forward, for the y-axis is left, and for the z-axis is cranial. We then replaced all scalars (ω_z, $\hat{\omega}_z$, α_{ω_z}, $\hat{\alpha}_{\omega_z}$, and e) with 3-dimensional vectors ($\vec{\omega}$, $\hat{\vec{\omega}}$, $\vec{\alpha}_\omega$, $\hat{\vec{\alpha}}_\omega$, and $\vec{e}$), with each component representing activity along the corresponding axis [x y z]. We also replaced the unity operators of the scalar model with 3×3 identity matrices ($I_{3\times3}$) and replaced the semicircular canal transfer function with a 3×3 transfer function matrix. Figure 5 shows a detailed block diagram representation of this 3-dimensional model.

Body dynamics and sensory dynamics. To avoid mathematical cross-coupling and to keep the parameters easily identified and interpreted, we assumed that the semicircular canals were mutually orthogonal, dynamically identical, and aligned with the x-, y-, and z-axes of the head:[4]

$$\frac{\vec{\alpha}_\omega(s)}{\vec{\omega}(s)} = S_{scc}(s) = \begin{bmatrix} scc(s) & 0 & 0 \\ 0 & scc(s) & 0 \\ 0 & 0 & scc(s) \end{bmatrix}, \quad [7]$$

where $scc(s)$ is the transfer function shown in equation 1.

Since three-dimensional rotation will, in general, constantly change the orientation of the gravitational force ($\vec{g}$), we also need to represent this physical effect. If we know the initial orientation of gravity ($\vec{g}_o$), and we impose an angular disturbance ($\vec{\omega}$), we must use rotational kinematics (for example, rotation matrices or quaternions) to keep track of the relative orientation of gravity. This physical effect is represented as part of the body dynamics ($\int \vec{\omega}\, dt \rightarrow \vec{g}$) shown in Figure 5. The actual calculations were implemented via a quaternion integration (40,41).

Since we added gravity to the three-dimensional model, we must also represent the dynamics of the otolith organs. The otolith organs were represented by a diagonal transfer function:[5]

$$\frac{\vec{\alpha}_f(s)}{\vec{f}(s)} = S_{oto}(s) = \begin{bmatrix} oto(s) & 0 & 0 \\ 0 & oto(s) & 0 \\ 0 & 0 & oto(s) \end{bmatrix}. \quad [8]$$

Since we limited the inputs to less than 1 Hz, the otolith transfer function was approximated as unity:[6]

$$oto(s) = 1. \quad [9]$$

Therefore,

$$\frac{\vec{\alpha}_f(s)}{\vec{f}(s)} = S_{oto}(s) = \begin{bmatrix} 1 & 0 & 0 \\ 0 & 1 & 0 \\ 0 & 0 & 1 \end{bmatrix} = I_{3\times3}. \quad [10]$$

Internal model of body dynamics and sensory dynamics. The internal model of both the body dynamics and the sensory dynamics was assumed to be consistent with the actual dynamics. The matrix transfer function of the internal semicircular canal model thus had a form similar to that of equation 7:

[4]Anatomical accuracy may easily be provided by changing the transfer function matrix from the diagonal form to one which truly represents the geometry of the semicircular canals. The internal model of the semicircular canals and the feedback gain matrix (K) would require analogous changes.

[5]This representation of the otolith organs assumed that the sensory afference from the two otolith organs, the utricle and the saccule, is centrally combined to yield a three-dimensional representation of gravitoinertial force. Some evidence suggests that utricular and saccular information may be processed differently. This might be simulated by changing weights in the feedback gain matrix (K).

[6]More complicated and accurate transfer functions (39) for the otoliths were utilized in early versions of the model and did not qualitatively affect the model response.

$$\frac{\hat{\bar{\alpha}}_\omega(s)}{\hat{\bar{\omega}}(s)} = \hat{S}_{scc}(s)$$

$$= \begin{bmatrix} s\hat{c}c(s) & 0 & 0 \\ 0 & s\hat{c}c(s) & 0 \\ 0 & 0 & s\hat{c}c(s) \end{bmatrix}, \quad [11]$$

with equation 2 yielding the appropriate transfer function for each $s\hat{c}c(s)$.

To keep the internal model similar to the true dynamics, we also included a mechanism by which the relative orientation of estimated gravity ("gravity storage") is rotated. Similar to the actual body dynamics calculations, we implemented a quaternion integrator[7] $\left(\int \hat{\bar{\omega}}\, dt \rightarrow \hat{\bar{g}}\right)$ to represent this hypothesized neural process.

We also assumed that the internal otolith model is an accurate representation of the true otolith dynamics. Therefore, similar to equation 10:

$$\frac{\hat{\bar{\alpha}}_f(s)}{\hat{\bar{f}}(s)} = \hat{S}_{oto}(s) = I_{3\times 3}. \quad [12]$$

Error calculations. Three error vectors are calculated in this multidimensional representation. The angular velocity error ($\vec{e}_\omega$) represents the difference between the actual semicircular canal afference and the expected semicircular canal afference. Two of the error vectors ($\vec{e}_a$ and $\vec{e}_f$) represent specific aspects of the difference between the actual otolith afference and the expected otolith afference. The linear acceleration error ($\vec{e}_a$) represents the vector difference between the actual otolith afference and the expected otolith afference, while the gravitoinertial force (GIF) rotation error ($\vec{e}_f$) represents the rotation required to bring the otolith measurement of GIF into alignment with the centrally estimated otolith measurement of GIF. Mathematical and physical explanations for each of these errors follows.

The angular velocity error vector ($\vec{e}_\omega$) has three components, each representing an error between the actual semicircular canal afference ($\bar{\alpha}_\omega$) and the expected semicircular canal afference ($\hat{\bar{\alpha}}_\omega$) along one of the three axes. This error is calculated via vector subtraction:

$$\vec{e}_\omega = \vec{\alpha}_\omega - \hat{\bar{\alpha}}_\omega. \quad [13]$$

Similarly, the linear acceleration error ($\vec{e}_a$) has three components, each representing an error between the actual otolith afference ($\vec{\alpha}_f$) and the expected otolith afference ($\hat{\bar{\alpha}}_f$) along one of the three axes. This error is also calculated via vector subtraction:

$$\vec{e}_a = \vec{\alpha}_f - \hat{\bar{\alpha}}_f. \quad [14]$$

Linear acceleration errors might result from linear acceleration or from accumulated errors in the estimation of gravity.

We postulated that the CNS might adjust its estimate of gravity based on the difference between the actual and expected otolith input. This was accomplished by implementing a GIF rotation error ($\vec{e}_f$), which represents the rotation (direction and magnitude) required to align the otolith measurement of gravitoinertial force ($\vec{\alpha}_f$) with the centrally estimated otolith measurement of gravitoinertial force ($\hat{\bar{\alpha}}_f$). We used a cross product to compute the direction of the rotation by calculating a unit vector that is perpendicular to the plane containing $\vec{\alpha}_f$ and $\hat{\bar{\alpha}}_f$:

$$\frac{\vec{e}_f}{|\vec{e}_f|} = \frac{\vec{\alpha}_f \times \hat{\bar{\alpha}}_f}{|\vec{\alpha}_f \times \hat{\bar{\alpha}}_f|}. \quad [15]$$

We used a dot product to compute the magnitude of the rotation:

$$|\vec{e}_f| = \cos^{-1}\left(\frac{\vec{\alpha}_f}{|\vec{\alpha}_f|} \cdot \frac{\hat{\bar{\alpha}}_f}{|\hat{\bar{\alpha}}_f|}\right). \quad [16]$$

The mathematics make the GIF rotation error look more complicated than it is. Physi-

[7]The quaternion integration is not essential for this model to function properly. Any method which uses angular velocity information to rotate the central estimate of gravity is appropriate. We also implemented this rotation using $d\bar{g}/dt = \bar{\omega} \times \bar{g}$. No qualitative differences in the model predictions were observed.

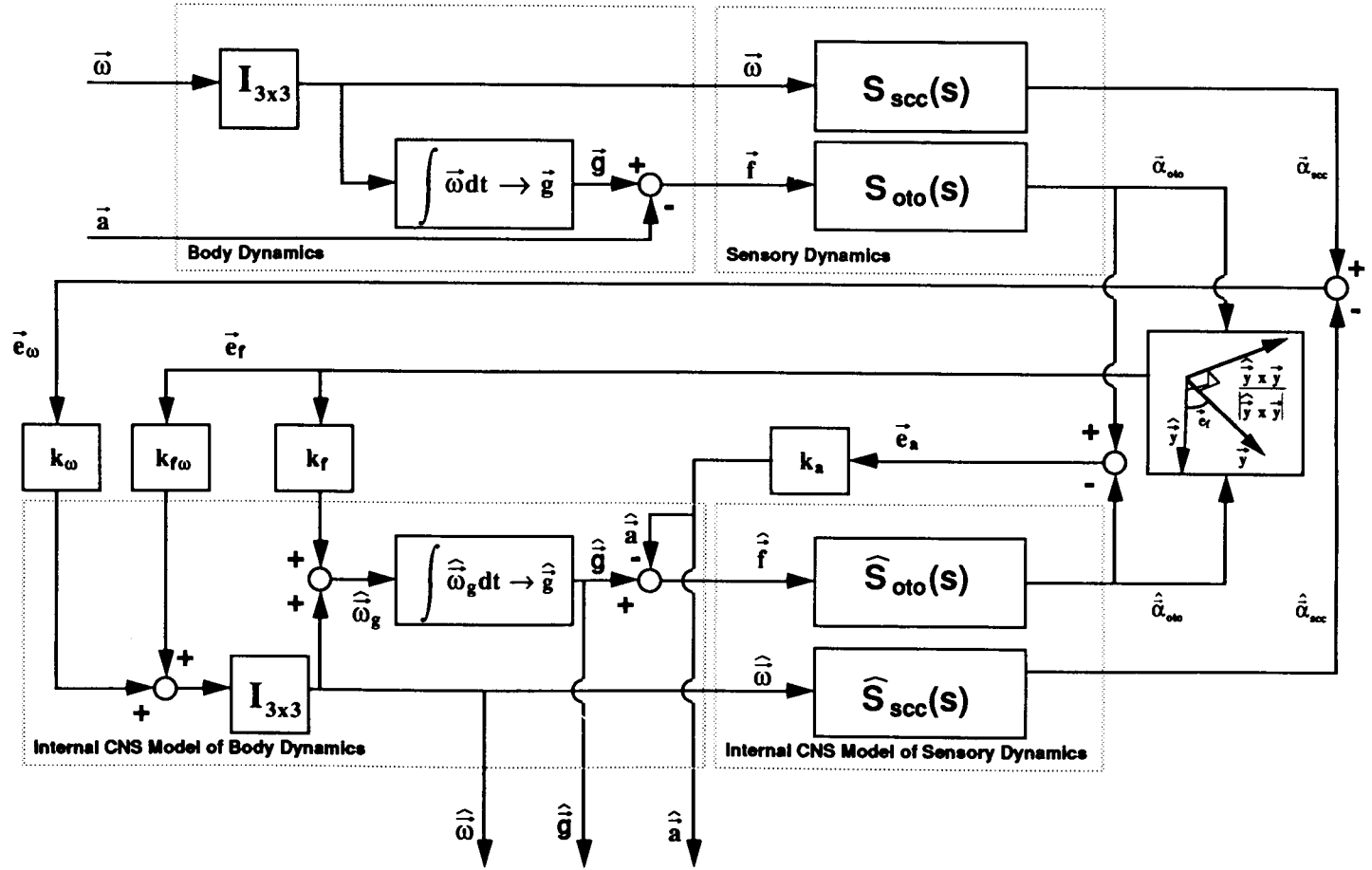

Figure 5. Three-dimensional sensory conflict model. The inputs to the system are three-dimensional angular velocity ($\vec{\omega}$) and three-dimensional linear acceleration ($\vec{a}$). To implement the three-dimensional nature of the model a 3 × 3 identity matrix is included as part of the body dynamics, a 3 × 3 semicircular canal transfer function matrix ($S_{scc}(s)$) represents the three dimensional semicircular canal dynamics, and a 3 × 3 otolith transfer function matrix ($S_{oto}(s)$) represents the three dimensional otolith dynamics. Three dimensional angular velocity will, in general, constantly change the orientation of the gravitational force, and this physical effect is represented as part of the body dynamics ($\int \vec{\omega}\, dt \rightarrow \vec{g}$). The internal model of the dynamics is essentially veridical with the actual dynamics. Four feedback gains (k_ω, $k_{f\omega}$, k_f, and k_a) multiply the sensory conflict errors ($\vec{e}_\omega$, $\vec{e}_f$, and $\vec{e}_a$) to yield the inputs to the internal model of body dynamics. The model outputs are central estimates of angular velocity ($\hat{\vec{\omega}}$), gravity ($\hat{\vec{g}}$), and linear acceleration ($\hat{\vec{a}}$).

cally, the GIF rotation error ($\vec{e}_f$) is simply the rotation that aligns the otolith measurement of gravitoinertial force ($\vec{\alpha}_f$) with the centrally estimated otolith measurement of gravitoinertial force ($\hat{\vec{\alpha}}_f$).

Error feedback. Four constant scalar feedback gains[8] (k_ω, k_a, k_f, and $k_{f\omega}$) are used to "steer" the central estimates ($\hat{\vec{a}}$, $\hat{\vec{g}}$, $\hat{\vec{\omega}}$) toward values that minimize the sensory conflict errors ($\vec{e}_\omega$, $\vec{e}_a$, $\vec{e}_f$) and represent the *only* free parameters in this model. The angular velocity feedback gain (k_ω) scales the angular velocity error ($\vec{e}_\omega$) and feeds it back to the central estimator of angular velocity ($\hat{\vec{\omega}}$). The linear acceleration feedback gain (k_a), likewise, scales the linear acceleration error ($\vec{e}_a$) to feed it back to the central estimator of linear acceleration ($\hat{\vec{a}}$). The GIF feedback gain (k_f) scales the GIF rotation error ($\vec{e}_f$) to feed it back to the central estimator for the direction of gravity ($\hat{\vec{g}}$), while the remaining feedback gain ($k_{f\omega}$) also scales the GIF rotation error ($\vec{e}_f$) to feed it back to the central estimator of angular velocity ($\hat{\vec{\omega}}$). Figure 5 shows how each of these feedback gains fits into the overall structure of the model.

The angular velocity error feedback gain (k_ω) determines how much the semicircular canal error ($\vec{e}_\omega$) influences the central estimate of angular velocity. As shown previously for the velocity storage model (equations 3–6), the response time constant and gain directly depend on this gain. In order to yield adequate velocity storage during rotations about an earth-vertical axis, the feedback gain was fixed at 3.0 [(°/s)/(°/s)]. With an assumed semicircular canal time constant of 5.7 seconds, this yielded a dominant time constant of 22.8 seconds and a gain of 0.75 (Figure 4), which is consistent with monkey responses.

The linear acceleration error gain (k_a) determines how much the linear acceleration error ($\vec{e}_a$) influences the central estimate of linear acceleration. For all of the presented simulations, the acceleration feedback gain was fixed at −0.9. This value indicates that the magnitude of the central estimate of linear acceleration is 90% of the magnitude of the difference between the otolith afference and the expected otolith afference. This value must have a magnitude less than 1 to remain stable, while the negative sign is required to transform force as detected by the otoliths into acceleration. The magnitude of the gain was chosen to be near one so that a large part of the linear acceleration error ($\vec{e}_a$) yielded a central estimate of linear acceleration ($\hat{\vec{a}}$).

The GIF feedback gain (k_f) determines how much the GIF rotation error ($\vec{e}_f$) induces the internal sense of gravity to align with the otolith measured gravitoinertial force, without inducing a change in the central estimate of angular velocity. The gain was fixed at a value of 2.0 [(°/s)/degrees]. The value of this parameter was not critical to any of these simulations and was varied between 0.01 and 10.0 without having any qualitative effects. We included this gain because it allows the central estimate of angular velocity ($\hat{\vec{\omega}}$) to be dissociated from the central estimate of tilt ($\hat{\vec{g}}$).

The remaining feedback gain ($k_{f\omega}$) was critical to the success of the model. It determines how much the GIF rotation error ($\vec{e}_f$) influences the central estimate of angular velocity ($\hat{\vec{\omega}}$). As the GIF rotation error increases, this error induces an estimate of self-rotation that tends to align the central estimate of gravity ($\hat{\vec{g}}$) with the otolith measure of gravitoinertial force ($\vec{\alpha}_f$). This gain was fixed at 20.0 [(°/s)/degrees]. This value was required to yield large steady-state rotational responses during OVAR stimulation and rapid shifts in the axis of eye rotation following postrotatory tilt. Larger values yielded larger bias components and smaller decay components during OVAR and faster axis shifts following postrotatory tilt, while smaller values had the opposite affect.

Model Predictions

The following simulations were implemented using Extend™, a dynamic systems

[8]By using scalar gains we implicitly assumed that rotations around and accelerations along the x-, y-, and z-axes are equivalent. Experimentation has shown that this is not always true. Replacing each of the scalar gains with a 3-component vector would provide the freedom to model these differences.

modeling software package, on a Macintosh™ computer. Simulations used simple trapezoidal integration with a fixed time increment of 0.005 seconds. For our multidimensional simulations, we chose two paradigms that stimulate both the otolith organs and the semicircular canals, and therefore require that the signals from these sensory systems be merged. In postrotational tilt, static otolith cues affect the postrotatory response normally induced by the semicircular canals' cues, and with off-vertical axis rotation (OVAR), dynamic otolith cues induce both static ("bias") and dynamic ("modulation") components.

Postrotational Tilt

Benson (42) showed the dramatic effect that tilt has on the postrotatory response of humans by demonstrating that the time constant of the horizontal VOR (HVOR) response is reduced following postrotational tilt. We have confirmed this result in the squirrel monkey and, using three-dimensional recording techniques, also showed that the axis of eye rotation shifted toward alignment with gravity following the postrotatory tilt (21). For purposes of a qualitative comparison with the computer simulations, these two characteristics, a shortened horizontal time constant and a shift in the axis of eye rotation, characterize the experimentally observed responses.

Modeling results. We simulated postrotational tilt after constant velocity yaw rotation of 100°/s about an earth-vertical axis. The simulated subject was decelerated to a stop in one second after the semicircular canal responses had decayed to near zero (50 seconds). Immediately after stopping, the subject was rolled 45 degrees to the left, with a peak angular roll velocity of 45 degrees per second. The simulated tilt was completed in 2 seconds (Figure 6A).

The model's central estimates of angular velocity and linear acceleration for this stimulus are shown in Figure 6, Panels B and C, respectively. The model predicts that 1) the central estimate of yaw velocity ($\hat{\omega}_z$) shows an exponential decay once the steady-state stimulus velocity is reached, and an opposite postrotatory response before the postrotatory tilt; 2) the central estimate of yaw velocity ($\hat{\omega}_z$) shows a dramatic decrease immediately following the postrotatory tilt; 3) a central estimate of pitch angular velocity ($\hat{\omega}_y$) builds up immediately following the tilt and decays to zero with a time course similar to the yaw response; 4) the central estimate of roll rotation ($\hat{\omega}_x$) responds to the roll angular velocity stimulation and then develops a very small roll estimate, which decays to zero; and 5) small central estimates of linear acceleration ($\hat{a}$) occur, which exponentially decay toward zero more rapidly than the angular velocity estimates.

The central estimate of gravity is correctly aligned with the body's z-axis throughout the rotation (Figure 6D). During the postrotatory tilt, the central estimate of gravity rapidly tilts, due to the influence of the canals, yielding a central estimate of gravity with the steady-state magnitude of the y- and z-components equal to .707 *g*'s (tilt equals 45°). A transient x-component of gravity gradually built up to an amplitude of 0.16 *g*'s following the postrotatory tilt.

The predicted VOR responses are shown in Figure 6, Panel E. (Recall that we assumed that the slow phase velocity of the compensatory angular VOR is exactly opposite the central estimate of angular velocity.) The simulated HVOR response is dominated by a compensatory response to the central estimate of yaw velocity, but also includes a compensatory response to the central estimate of interaural acceleration ($\hat{a}_y$). Close examination of the model predictions showed that the horizontal postrotatory response decayed faster than the perrotatory response and the upright postrotatory response. This was primarily due to the initial rapid decay that occurred immediately following the tilt. The simulated vertical VOR (VVOR) response is dominated by a compensatory response to the central estimate of pitch velocity, but also includes a small compensatory response to the central estimate of z-axis acceleration ($\hat{a}_z$). This VVOR shifted the axis of eye rotation toward alignment with

gravity. The simulated torsional VOR (TVOR) response is dominated by a compensatory response to the angular velocity stimulation during the roll tilt, but a very small decaying torsional response was also evident. The model predicted both response components (rapid decay and axis shift), which characterize the experimentally observed postrotatory responses in the monkey, although the decay following the postrotatory tilt was not as rapid as indicated by the experiments. [See previous paper (21).]

Physical explanation of results. After deceleration, the horizontal semicircular canals signal a rotation in the counterclockwise direction (α_{ω_z}). This produces a large angular velocity error (e_{ω_z}), which, when weighted by the angular velocity feedback gain (k_ω), quickly drives the central estimate of z-axis angular velocity ($\hat{\omega}_z$) toward the amount indicated by the horizontal canals. During the roll, the vertical canals detect this angular rotation (α_{ω_x}), and acting through the same paths, create a transient central estimate of angular velocity about the x-axis ($\hat{\omega}_x$). The estimate of head roll velocity gets "integrated" to produce a change in the estimated direction of gravity ($\hat{\vec{g}}$) that essentially continues to align with gravity as detected by the otoliths ($\hat{\vec{\alpha}}_f$).

However, following the tilt, the strong postrotational semicircular canal afferent signal ($\vec{\alpha}_\omega$), which is no longer aligned with gravity, acts to rotate the estimate of gravity ($\hat{\vec{g}}$) away from the true vertical and thus generates a GIF rotation error ($\vec{e}_f$) and a linear acceleration error ($\vec{e}_a$). The linear acceleration error, scaled by k_a, results in a reinterpretation of a portion of the otolith afference as indicating linear acceleration ($\hat{\vec{a}}$). The GIF rotation error, scaled by $k_{f\omega}$, primarily induces a y-component of the central estimate of angular velocity ($\hat{\omega}_y$) that shifts the central estimate of rotation toward alignment with gravity. In this simulation, this feedback gain ($k_{f\omega}$) is large enough to produce an axis shift that keeps the central estimate of rotation ($\hat{\vec{\omega}}$) essentially stable in space.

The acceleration and gravity errors disappear with an apparent time constant shorter than that of angular velocity storage, indicating that the dynamics are somewhat unrelated, though obviously dependent on the central estimate of angular velocity. It is the interaction of gravity storage ($\hat{\vec{g}}$) with velocity storage ($\hat{\vec{\omega}}$) that leads to the spatial stability of the central estimate of angular velocity when the head is tilted.

Off-Vertical Axis Rotation (OVAR)

A number of studies have shown that constant velocity OVAR induces an HVOR response in humans that contains three components: an exponential decay, a constant bias, and a sinusoidal modulation (23,24). These results have been qualitatively confirmed in monkeys (25) with the bias component predominant. A later study (26) showed that the VVOR response also had a modulation component. More recently, the same group presented data indicating that the TVOR also has a modulation component (43). For purposes of a qualitative comparison with the computer simulations, these five characteristics (modulation components for HVOR, VVOR, and TVOR; horizontal bias component; and partial exponential decay for horizontal response) appear to characterize the observed responses in monkeys.

Modeling results. Figure 7 shows the OVAR simulation with a constant velocity yaw rotation of 100°/s toward the left about an axis that was tilted 45 degrees from the vertical. The simulated central estimate of angular velocity is shown in Figure 7, Panel B. Once constant velocity was attained, the z-axis angular velocity estimate ($\hat{\omega}_z$) began to decay and eventually reached a steady-state angular velocity of 64°/s. Oscillations in the central estimates of x-axis (roll-$\hat{\omega}_x$) and y-axis (pitch-$\hat{\omega}_y$) angular velocity were also evident, with the frequency of oscillation corresponding to the rotation rate of the subject. The peak value of the oscillations was just less than 20°/s, and the y-axis response led the z-axis response by 90 degrees. Thus, the instantaneous rotation axis seems to cone around the simu-

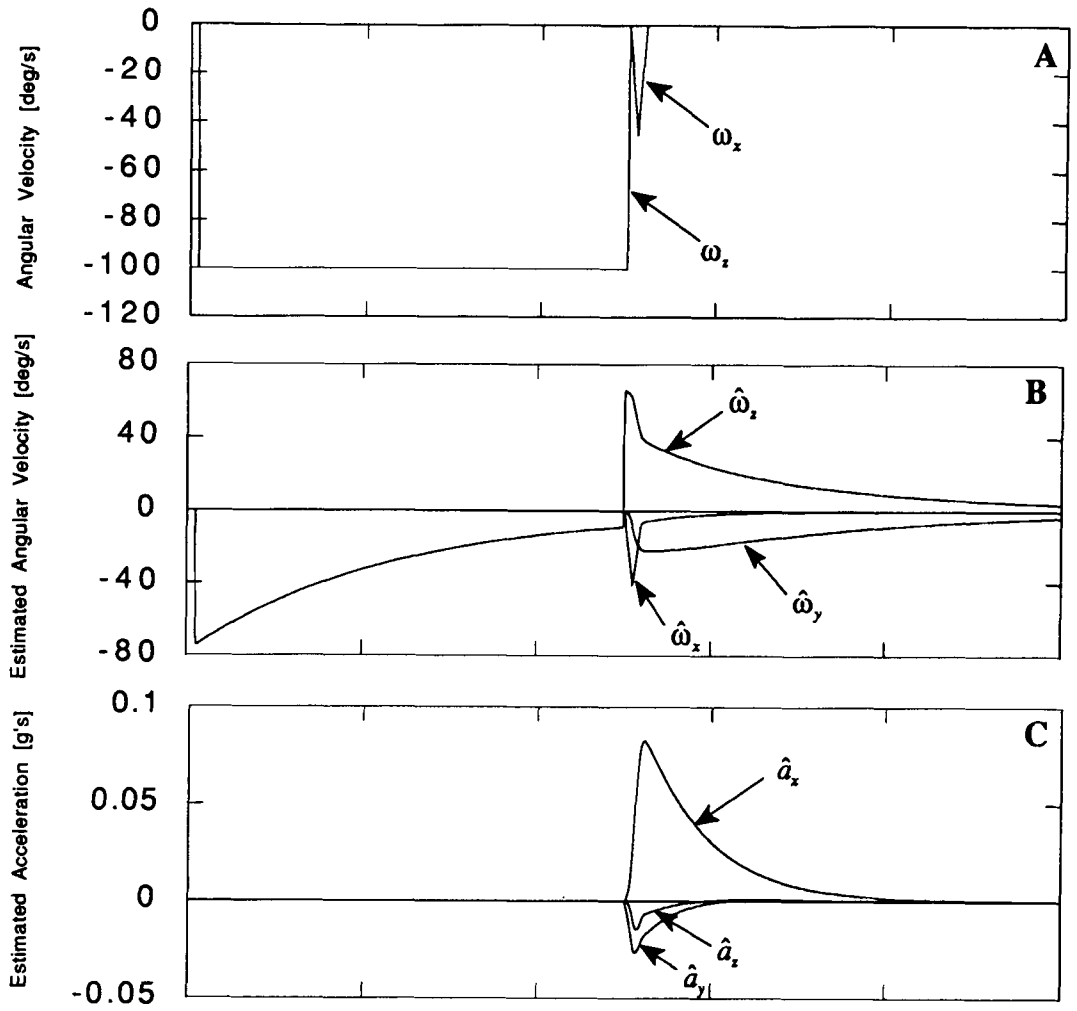

Figure 6. "Postrotatory tilt"-model predictions. Panel A shows the yaw velocity trapezoid (ω_z), followed by a roll (ω_x), which results in a 45 degree tilt to the left. Panel B shows predicted central estimates of angular velocity, Panel C shows the predicted central estimates of linear acceleration, and Panel D shows the central estimates of gravity. Panel E shows the VOR response predicted to compensate for the central estimates shown in Panels B and C. (*Figure continues on facing page.*)

lated subject with a cone angle of 17 degrees [$\tan^{-1}(19.7/64.0)$]. By simply integrating the oscillatory central estimate of angular velocity we can determine that the tilt with respect to the z-axis associated with this angular velocity is approximately 11 degrees.

The x- and y-components of the central estimate of gravity also develop oscillations at the frequency of rotation (Figure 7, Panel D). In the steady-state the x- and y-components are 90° out of phase and have a peak magnitude of 0.701 g, while the z-component has a steady-state value of 0.712 g. Therefore, the steady-state tilt with respect to the z-axis is 44.5 degrees [$\tan^{-1}(0.701/0.712)$], with the direction of the estimated tilt, like the real tilt, oscillating about the subject. This clearly shows that tilt is not simply the integral of angular velocity, since the estimated tilt (44.5 degrees) is not the same as the integral of the angular velocity (11°/s) as calculated previously. Therefore, the central estimates of

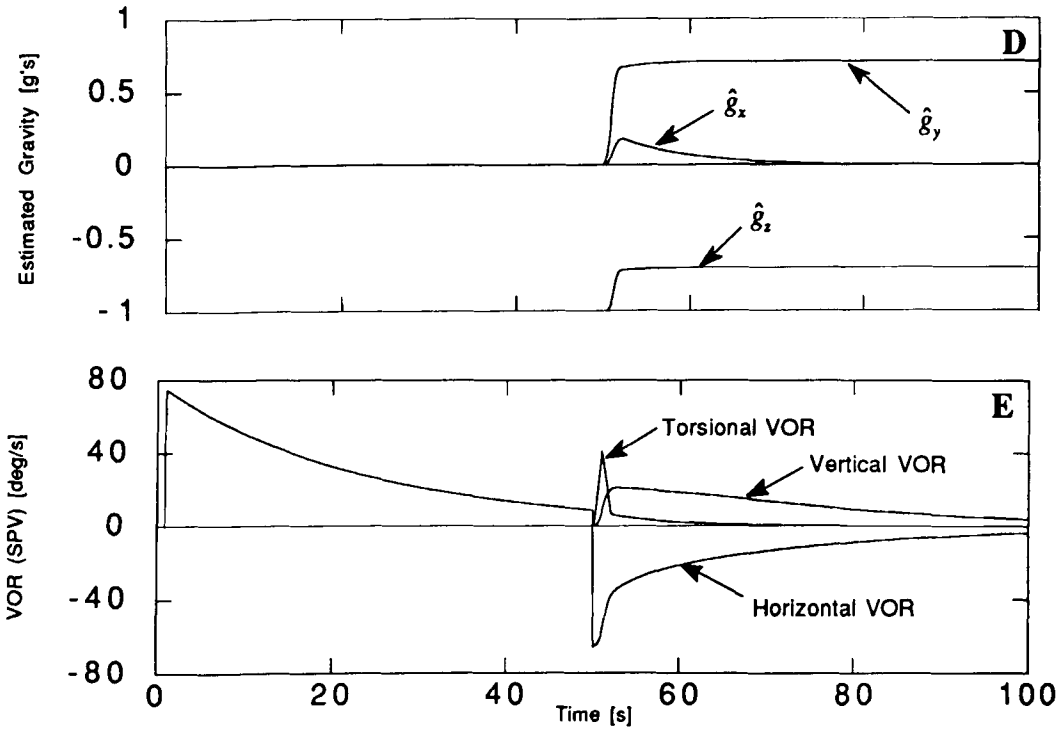

Figure 6 continued.

tilt ($\hat{\vec{g}}$) and angular velocity ($\hat{\vec{\omega}}$) are somewhat dissociated.

The model further predicted that oscillations occur in the central estimates of linear acceleration (Figure 7, Panel C) for the x-direction (naso-occipital) and y-direction (interaural). Again, the frequency of the oscillations corresponds to the rate of rotation, and the oscillating linear acceleration estimates reached a peak of 0.086 g's. The interaural estimate ($\hat{a}_y$) led the naso-occipital estimate ($\hat{a}_x$) by 90 degrees. Doubly integrating these components to determine linear displacement corresponds to a circular head motion with a radius of 0.28 m.

The VOR responses predicted from these central estimates are shown in Figure 7, Panel E. The simulated horizontal VOR response was dominated by a compensatory response to the central estimate of yaw velocity, but also included a small compensatory response to the oscillating central estimate of interaural acceleration ($\hat{a}_y$). The horizontal VOR response showed an exponential decay toward a bias level and also showed a small modulation. This is qualitatively similar to the monkey responses. The simulated vertical VOR response was dominated by a compensatory response to the oscillating central estimate of pitch velocity ($\hat{\omega}_y$), but also included a small compensatory response to the oscillating central estimate of z-axis acceleration ($\hat{a}_z$). The simulated torsional VOR response was a compensatory response to the oscillating central estimate of roll velocity. Surprisingly, this model qualitatively predicted all of the components that characterize an OVAR response in the monkey.

Physical explanation of results. A key to understanding the steady-state responses in Figure 7 is to realize that many of the estimated state vectors become fixed in magnitude and direction with respect to inertial space, and that the oscillatory behavior of the x and y components results from the rotation of the

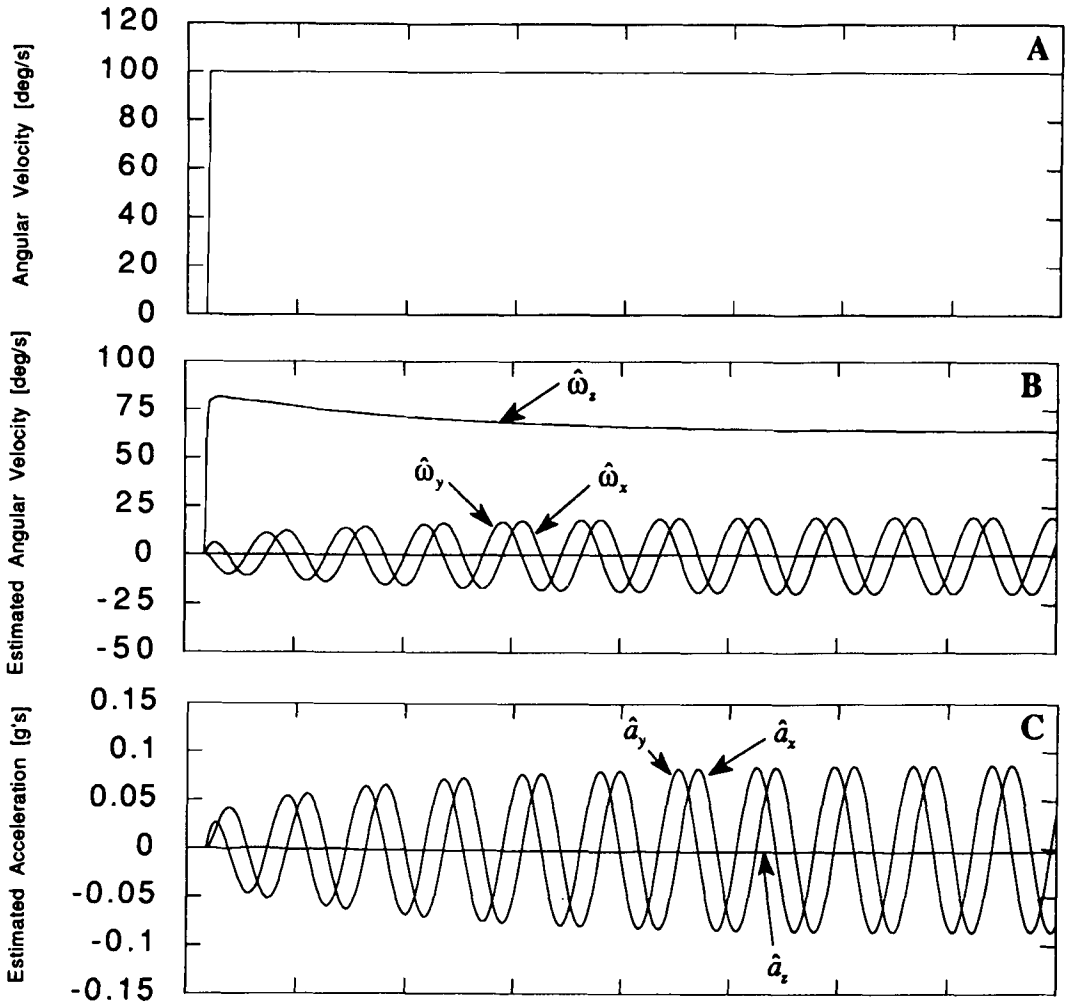

Figure 7. "OVAR"-model predictions. Panel A shows the trapezoidal yaw stimulation that is applied about an axis tilted 45 degrees from the vertical. Panel B shows the central estimates of angular velocity, C shows the central estimates of linear acceleration, D shows the central estimates of gravity. Panel E shows the VOR response predicted to compensate for the central estimates shown in Panels B and C. (*Figure continues on facing page.*)

subject about these fixed vectors. With no otolith dynamics, the otolith afference vector ($\vec{\alpha}_f$) is spatially fixed as it physically tracks the real g vector. The central estimate of linear acceleration ($\hat{a}$) can be observed to be a phasor that rotates at the stimulus frequency in the plane of true rotation and therefore is also spatially constant. Since the central estimate of linear acceleration was defined to be the product of a fixed feedback gain (k_a) and the linear acceleration error ($\vec{e}_a$), the linear acceleration error must also be spatially constant. Therefore, the expected otolith afference ($\hat{\vec{\alpha}}_f$) must also be spatially fixed. If both the actual and expected otolith afference are fixed in space, the GIF rotation error ($\vec{e}_f$) must also be fixed. Similarly, the central estimates of gravity ($\hat{\vec{g}}$) and gravitoinertial force ($\hat{\vec{f}}$) are spatially constant.

As previously stated, gravity as detected by the otoliths ($\hat{\vec{\alpha}}_f$) is assumed to be earth vertical, and because the direction of the GIF

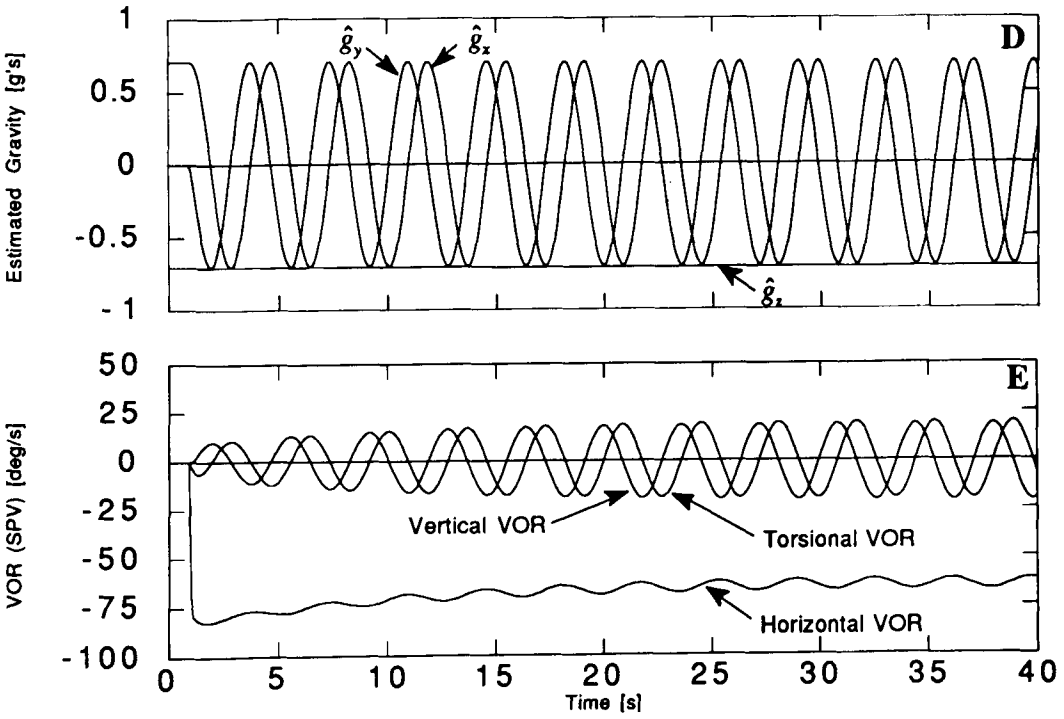

Figure 7 continued.

error ($\vec{e}_f$) is defined by a cross product, the GIF error must lie in a horizontal plane. Since the body is tilted 45°, one component of this constant error lies along the z-axis of the body, and when scaled by $k_{f\omega}$ yields the z-axis bias component of the central estimate of angular velocity ($\hat{\omega}_z$). The remaining component of the GIF rotation error is perpendicular to the body z-axis and, because it is fixed in space, rotates with respect to the body once per revolution of the subject. Scaled by $k_{f\omega}$, this component of the GIF rotation error induces oscillating central estimates ($\hat{\omega}_x$ and $\hat{\omega}_y$) of angular velocity. Because this oscillatory stimulus is within the dynamic range of the canals, the oscillatory x and y components of the central estimate of angular velocity ($\hat{\vec{\omega}}$) are partially canceled by the semicircular canal error vector ($\vec{e}_\omega$) scaled by k_ω. Analogous arguments explain the oscillating x and y components of the central estimate of linear acceleration ($\hat{\vec{a}}$) and the oscillating x and y components of the central estimate of gravity ($\hat{\vec{g}}$).

Conclusion

We have implemented a fundamentally novel model, using ideas that were previously only present in a qualitative form (12–20). These qualitative hypotheses were rigorously implemented using system theory in a natural, physically meaningful way. By representing these fundamental physical principles in a mathematical framework, we have qualitatively captured the essential vestibulo-ocular characteristics of three-dimensional velocity storage, postrotatory tilt, and OVAR. This was accomplished with only four free parameters, all of which were fixed throughout the simulations. This contrasts with previous models, which have relied on variations in system parameters to yield the desired predictions.

Despite its successes, the model has some limitations. For example, the model does not yet include the visual system or, for that matter, any sensory system other than the vestibular system. The current model is also only

valid for passive motion. The framework allows for extension to active motion paradigms, but this portion of the model has yet to be developed.

Despite these restrictions, for the three test cases shown, this modeling approach qualitatively characterizes the observed responses and predicts a number of experimentally observed responses that we did not explicitly build into the model. For example, the axis shift following postrotatory tilt (Figure 6, panels B and E) appeared although no portion of the model was explicitly included to predict this effect. We also observed experimentally verified oscillations in the x ($\hat{\omega}_x$) and y components ($\hat{\omega}_y$) of angular velocity (Figure 7), which were not built into the model in any way (for example, variation of system parameters). These surprising emergent properties in a 1-g environment encourage us to extend this model to more fully test its limitations and capabilities.

Acknowledgments—This research was supported by NASA contracts NASW-3651, NAG2-445, NAS9-16523, the NASA Graduate Student Researchers Program, and the GE Forgivable Loan Fund. We also thank Sherry Modestino for her assistance in many phases of this research, Brad McGrath for providing an early version of the quaternion integrator, and Imagine That! for supplying the modeling program "Extend™" to the Man-Vehicle Laboratory.

REFERENCES

1. Robinson DA. Vestibular and optokinetic symbiosis: an example of explaining by modeling. In: Baker R, Berthoz A, eds. Control of gaze by brain stem neurons, developments in neuroscience, vol 1. Amsterdam: Elsevier/North-Holland Biomedical Press; 1977:49–58.
2. Raphan T, Matsuo V, Cohen B. A velocity storage mechanism responsible for optokinetic nystagmus (OKN), optokinetic after-nystagmus (OKAN) and vestibular nystagmus. In: Baker R, Berthoz A, eds. Control of gaze by brain stem neurons. Amsterdam: Elsevier/North-Holland Biomedical Press; 1977: 37–47.
3. Borah J, Young LR, Curry RE. Optimal estimator model for human spatial orientation. Ann NY Acad Sci. 1988;545:51–73.
4. Kalman RE, Bucy RS. New results in linear filtering and prediction theory. J Basic Eng Trans. ASME Ser D. 1961;83:95–108.
5. Dichgans J, Schmidt CL, Graf W. Visual input improves the speedometer function of the vestibular nuclei in the goldfish. Exp Brain Res. 1973;18:319–22.
6. Henn V, Young LR, Finley C. Vestibular nucleus units in alert monkeys are also influenced by moving visual fields. Brain Res. 1974;71:144–9.
7. Waespe W, Henn V. Neuronal activity in the vestibular nuclei of the alert monkey during vestibular and optokinetic stimulation. Exp Brain Res. 1977;27: 523–38.
8. Hain TC. A model of the nystagmus induced by off vertical axis rotation. Biol Cybern. 1986;54:337–50.
9. Raphan T, Matsuo V, Cohen B. Velocity storage in the vestibulo-ocular reflex arc (VOR). Exp Brain Res 1979;35:229–48.
10. Raphan T, Cohen B. Multidimensional organization of the vestibulo-ocular reflex (VOR). In: Keller E, Zee D, eds. Adaptive processes in visual and oculomotor systems. 1986:285–92.
11. Sturm D, Raphan T. Modeling the three dimensional structure of velocity storage in the vestibulo-ocular reflex (VOR). 1988; Proceedings of the 14th Bioengineering Conference (IEEE).
12. Oman CM. A heuristic mathematical model for the dynamics of sensory conflict and motion sickness. Acta Otol. 1982;(Suppl):392.
13. von Uexkull, J. Theoretische Biologie. Suhrkamp; 1926: 156–61;300–10.
14. Sperry RW. Neural basis of the spontaneous optokinetic response produced by vision inversion. J Comp Physiol Psychol. 1950;43:482–9.
15. von Holst E. Relations between the central nervous system and the peripheral organs. Brit J Anim Behav. 1954;2:89–94.
16. von Holst E. Aktive Leistungen der menschlichen Gesichtswahrnehmung. Studium Generale. 1957;10: 231–43.
17. Hein A, Held R. A neural model for labile sensorimotor coordinations. Biol Prototypes Synthetic Syst. 1961;1:71–4.
18. Held R. Exposure history as a factor in maintaining stability of perception and coordination. J Nerv Ment Dis. 1961;132:26–32.
19. Reason JT. Learning to cope with atypical force environments. In: Howe M, ed. Adult Learning. London: Wiley 1977:203–22.
20. Reason JT. Motion sickness adaptation: a neural mismatch model. J Royal Soc Med 1978;71:819–29.
21. Merfeld DM, Young LR, Paige GD, Tomko DL. Effect of post-rotatory tilt on 3-dimensional eye movements in monkeys. J of Vestibular Res. 1993;3:123–139.
22. Merfeld DM. Spatial orientation in the squirrel monkey: an experimental and theoretical investigation [Ph.D. Thesis]. Cambridge, Massachusetts: Massachusetts Institute of Technology; 1990.
23. Benson AJ, Bodin MA. Interaction of linear and angular accelerations on vestibular receptors in man. Aerospace Med. 1966;37:144–54.

24. Correia MJ, Guedry FE. Modification of vestibular responses as a function of rate of rotation about an earth-horizontal axis. Acta Otol. 1966;62:297-308.
25. Young LR, Henn VS. Nystagmus produced by pitch and yaw rotation of monkeys about non-vertical axes. Fortschr Zool. 1975;23:235-46.
26. Raphan T, Cohen B, Henn V. Effects of gravity on rotatory nystagmus in monkeys. Ann NY Acad Sci. 1981;374:44-55.
27. Graybiel A, Brown R. The delay in visual reorientation following exposure to a change in direction of resultant force on a human centrifuge. J Gen Psychol. 1951;45:143-50.
28. Young LR. Effects of linear acceleration on vestibular nystagmus. 3rd Symposium on the Role of the Vestibular Organs in Space Exploration. Washington, DC: US Government Printing Office; 1967; NASA SP-152:383-91.
29. Young LR. Cross coupling between effects of linear and angular acceleration on vestibular nystagmus. Bibl Ophthalmol. 1972;82:116-21.
30. Merfeld DM, Young LR, Paige GD, Tomko DL. Spatial orientation of the VOR to combined vestibular stimuli in squirrel monkeys. Acta Otol. 1991; 481(Suppl):284-92.
31. Schwarz U, Busettini C, Miles FA. Ocular responses to linear motion are inversely proportional to viewing distance. Science. 1989;245:1394-6.
32. Paige GD. Tomko DL. Eye movement responses to linear head motion in the squirrel monkey; I: Basic characteristics. J. Neurophysiol. 1991;65: 1170-2.
33. Paige GD, Tomko DL. Eye movement responses to linear head motion in the squirrel monkey; II: Visual-vestibular interactions and kinematic considerations. J Neurophysiol. 1991;65:1183-96.
34. Robinson DA. Integrating with neurons. Annu Rev Neurosci. 1989;12:33-45.
35. Viirre E, Tweed D, Milner K, Vilis, T. A reexamination of the gain of the vestibuloocular reflex. J Neurophysiol. 1990;56:439-50.
36. Sargent EW, Paige GD. The primate vestibulo-ocular reflex during combined linear and angular head motion. Exp Brain Res. 1991;87:75-84.
37. Luenberger DG. An introduction to observers. IEEE Trans Autom Control, 1971;AC-16:596-603.
38. Goldberg JA, Fernandez C. Physiology of peripheral neurons innervating semicircular canals of the squirrel monkey; II: Response to sinusoidal stimulation and dynamics of peripheral vestibular system. J Neurophysiol. 1971;34:661-75.
39. Fernandez C, Goldberg J. Physiology of peripheral neurons innervating the otolith organs of the squirrel monkey; III: Response dynamics. J Neurophysiol. 1976;39:996-1008.
40. Rolfe JM, Staples KJ. Flight simulation. Cambridge: Cambridge University Press; 1977.
41. Tweed D, Vilis T. Implications of rotational kinematics for the oculomotor system in three dimensions. J Neurophysiol. 1987;58:832-49.
42. Benson AJ. Modification of the per- and postrotational responses by the concomitant linear acceleration. In: 2nd Symposium on the Role of the Vestibular System in Space Exploration. Washington, DC: US Government Printing Office; NASA. 1966; SP-115:199-213.
43. Cohen B, Raphan T, Reisine H, Dai M. The otoliths generate nystagmus through the vestibulo-ocular reflex (VOR) [abstract]. Presented at the Barany Meeting in Tokyo, Japan. 1990 May 28-30.